

# Optical-spectrum-synthesizer design within an all-optical semiconductor gate to reduce waveform distortion induced by carrier-cooling relaxation at sub-Terahertz frequencies

Yoshiyasu Ueno, Ryouichi Nakamoto, Jun Sakaguchi, and Rei Suzuki<sup>\*)</sup>

Graduate School of Electronic Engineering, Univ. of Electro-Communications,  
1-5-1 Chofugaoka, Chofu, Tokyo 182-8585, Japan  
[ueno@ee.uec.ac.jp](mailto:ueno@ee.uec.ac.jp), <http://www.ultrafast.ee.uec.ac.jp>

<sup>\*)</sup> present affiliation: Hitachi Communication Technologies, Ltd.

**Abstract:** In frequency ranges above 200-300 GHz, the second slowest relaxation in the optical response (such as carrier-cooling relaxation having a time constant of 1-2 ps) of a semiconductor optical amplifier inside the conventional delayed-interference signal-wavelength converter (DISC) scheme is thought to *start the distortion* of all-optically gated waveforms. In this work, we design a digital optical-spectrum-synthesizer block that is part of the expanded DISC scheme. Our numerically calculated spectra, waveforms, and eye diagrams with assumed pseudorandom digital data pulses indicate that this synthesizer significantly removes strong distortion from the gated waveforms. A signal-to-noise ratio of 20 dB was obtained from our random-data eye diagram, providing proof of effectiveness in principle.

©2006 Optical Society of America

**OCIS codes:** (060.2330) Fiber optics communications; (120.5060) Phase modulation; (190.5970) Semiconductor nonlinear optics; (190.7110) Ultrafast nonlinear optics; (250.5980) Semiconductor optical amplifiers; (320.7080) Ultrafast devices; (320.7160) Ultrafast technology.

---

## References and links

1. J.P. Sokoloff, P.R. Prucnal, I. Glesk, and M. Kane, "A Tera-hertz optical asymmetric demultiplexer (TOAD)," *IEEE Photonics Technol. Lett.* **5**, 767-790 (1993).
2. K. Tajima, "All-optical switch with switch-off time unrestricted by carrier lifetime," *Jpn. J. Appl. Phys.* **32**, L1746-1749 (1993).
3. Y. Ueno, S. Nakamura, and K. Tajima, "Record low-power all-optical semiconductor switch operation at ultrafast repetition rates above the carrier cutoff frequency," *Opt. Lett.* **23**, 1846-1848 (1998).  
<http://ol.osa.org/abstract.cfm?id=37041>
4. K. Stubkjaer, "Semiconductor optical amplifier-based all-optical gates for high-speed optical processing," *IEEE J. Selected Topics in Quantum Electron.* **6**, 1428-1435 (2000).
5. Y. Ueno, S. Nakamura, and K. Tajima, "Nonlinear phase shifts induced by semiconductor optical amplifiers with control pulses at repetition frequencies in the 40-160 GHz range for use in ultrahigh-speed all-optical signal processing," *J. Opt. Soc. Am. B* **19**, 2573-2589 (2002).  
<http://josab.osa.org/abstract.cfm?id=70413>
6. Y. Liu, E. Tangdionga, Z. Li, H. de Waardt, A.M.J. Koonen, G.D. Khoe, H.J.S. Dorren, X. Shu, and I. Bennion, "Error-free 320-Gb/s SOA-based wavelength conversion using optical filtering," *Optical Fiber Communication Conference (OFC 2006)*, March 5-10, 2006, Anaheim, PDP28.
7. S. Nakamura, Y. Ueno, and K. Tajima, "Error-free all-optical demultiplexing at 336 Gb/s with a hybrid-integrated symmetric-Mach-Zehnder switch," *Optical Fiber Communication Conference (OFC 2002)*, March 17-22, 2002, Anaheim, Post-deadline Paper FD3.
8. Y. Ueno, S. Nakamura, and K. Tajima, "Spectral phase-locking in ultrafast all-optical Mach-Zehnder-type semiconductor wavelength converters," *Jpn. J. Appl. Phys.* **38**, L1243-1245 (1999).
9. J. Leuthold, D.M. Marom, S. Cabot, J.J. Jacques, R. Ryf, and C.R. Giles, "All-optical wavelength conversion using a pulse reformatting optical filter," *J. Lightwave Technol.* **22**, 186-192 (2004).

10. S. Nakamura, Y. Ueno, and K. Tajima, "Femtosecond switching with semiconductor-optical-amplifier-based Symmetric-Mach-Zehnder-type all-optical switch," *Appl. Phys. Lett.* **78**, 3929-3931 (2001).
11. Y. Lai, K.L. Hall, E.P. Ippen, and G. Eisenstein, "Short pulse gain saturation in InGaAsP diode laser amplifiers," *IEEE Photonics Technol. Lett.* **2**, 711-713 (1990).
12. J. Mork and A. Mecozzi, "Theory of the ultrafast optical response of active semiconductor waveguides," *J. Opt. Soc. Am. B* **13**, 1803-1816 (1996). <http://josab.osa.org/abstract.cfm?id=33873>
13. J. Mork, T.W. Berg, M.L. Nielsen, and A.V. Uskov, "The role of fast carrier dynamics in SOA-based devices," *IEICE Trans. Electron.* **E87-C**, 1126-1132 (2004).
14. M.L. Nielsen, J. Mork, R. Suzuki, J. Sakaguchi, and Y. Ueno, "Experimental and theoretical investigation of the impact of ultra-fast carrier dynamics on high-speed SOA-based all-optical switches," *Optics Express* **14**, 331-347 (2006). <http://oe.osa.org/abstract.cfm?id=86916>
15. Y. Ueno, M. Toyoda, R. Suzuki, and Y. Nagasue, "Modeling of the polarization-discriminating-symmetric-Mach-Zehnder-type optical-3R gate scheme and its available degree of random-amplitude-noise suppression," *Optics Express* **14**, 348-360 (2006). <http://oe.osa.org/abstract.cfm?id=86917>
16. K. Takiguchi, T. Kominato, H. Takahashi, T. Shibata, and K. Okamoto, "Flexible pulse waveform generation using a silica waveguide based spectrum synthesis circuit," *Optical Fiber Communication Conference (OFC 2004)*, Feb. 22-24, 2004, Los Angeles, CA, USA, paper no. TuI5.

## 1. Introduction

All-optical semiconductor gates, which generally consist of compact semiconductor optical amplifiers (SOAs), optical interferometers, and spectral band-pass filters, have been attracting attention since the early 1990s, because of their ultrahigh-frequency response, lower power consumption (compared to equivalent o-e-o-conversion systems), and functionalities [1-5]. Inside each gate, the SOA works actively as a source of instantaneous all-optical responses, while the interferometers and filters play optically passive roles. With regard to frequency, the most successful gate schemes to date have been the delayed-interference wavelength converter (DISC) [3] and the symmetric Mach-Zehnder (SMZ) demultiplexer [2]; Liu et al. recently achieved 320-Gb/s wavelength conversion with the DISC scheme [6], and Nakamura et al. have achieved 336-Gb/s 32:1 demultiplexing with the SMZ scheme [7]. In earlier designs and demonstrations of DISC and SMZ schemes in a frequency range below 200-300 GHz, the all-optical response of semiconductors has been assumed to have only a time constant; i.e., *the slowest relaxation time constant*, which is called the carrier lifetime or recovery time [2, 3, 5].

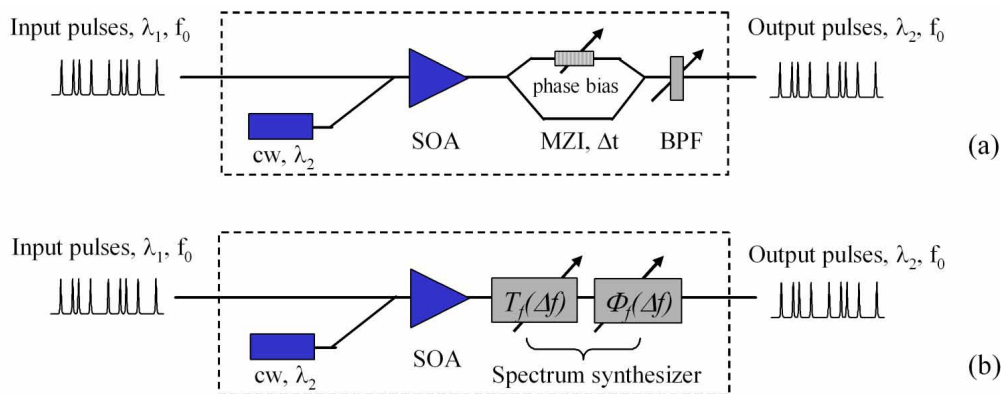


Fig. 1. Schematic views of the two alternative DISC schemes considered in this work. (a) conventional scheme and (b) expanded scheme with the optical spectrum synthesizer block,  $f_0$ : the frequency or the bitrate of the input.

In conventional DISC and SMZ designs under this first-order approximation, the optimum MZ interference removes most of the slow temporal components from the gated output waveforms. In the conventional DISC scheme (Fig. 1(a)), in particular, we can interpret this working principle (under the first-order approximation) in the frequency domain as well as in the time domain [8]; the MZ interferometer (MZI) works as an optical-

frequency-comb-like filter which removes most of the frequency-spectral components that would otherwise develop a slow trailing edge in the gated output waveforms. From this design viewpoint in the optical-frequency domain, the conventional combination of the MZI filter and the band-pass filter inside the DISC scheme was experimentally expanded by Leuthold, et al. to *one optical-spectrum synthesizer block* (Fig. 1(b)) which independently controls both the intensity and the phase of each spectrally resolved component ( $\Delta f = 40$  GHz) to improve the 40-Gb/s gated waveform quality [9].

In a frequency range above 200-300 GHz, though, *the second slowest relaxation* in the optical response of an SOA [10] may start to distort (or at least influence) the gated output waveforms; this second slowest relaxation originates from the cooling-down process of the quasi-Fermi electron distribution right after the electron temperature is raised (i.e., after carrier-heating occurs) by incoming ultra-short optical pulses [11-13]. The value of this carrier-cooling relaxation time constant is 1 to 2 ps [10]. More recently, Nielsen, Mork, and two of the present authors experimentally determined that a relatively small red-shift of the narrow band-pass filter's center-frequency position inside the DISC scheme improves its gated output waveforms and theoretically verified that this is an unexpectedly positive impact of the carrier-cooling relaxation [14]. The 320-Gb/s wavelength-conversion mentioned above [6] also seems to be physically supported by a similar combination of carrier-cooling-induced optical components and a red-shifted band-pass filter. Despite these observations of carrier-cooling-induced phenomena in an ultrafast DISC converter, to the best of our knowledge no optical spectrum synthesizer block of the type referred to above has been designed to take into account the second slowest relaxation and its time constant.

In this work, our goal was to design an optical spectrum synthesizer, using the expanded DISC scheme shown in Fig. 1(b), that can remove the second-slowest-relaxation-induced waveform distortion (independently from the MZI function that removes the slowest-relaxation-induced trailing components). As input optical signals, we have assumed clock pulses in the first step, and then pseudorandom-digital-data pulses in the second step. Our numerical results indicate that we can clearly remove the strong, second-slowest-relaxation-induced waveform distortion by optimizing the spectrum-synthesizer's complex spectral profiles.

## 2. Gate model

For the conventional DISC scheme (Fig. 1(a)), we used a model that has been used and experimentally verified [3, 5]. When each of the input optical pulses ( $\lambda_1$ ) propagates through the SOA and is amplified by the SOA, the carrier density in the SOA is instantaneously depleted and then recovers relatively slowly. This input-pulse-induced, saw-tooth-like evolution of the carrier density causes the co-propagating continuous wave (cw) probe light ( $\lambda_2$ ) to be both cross-phase modulated (XPM) and cross-gain modulated (XGM). When the cross-phase- and cross-gain-modulated probe light penetrates the asymmetric MZI, the probe light is split into two components. One of the two components is given a delay time  $\Delta t$ , and then the two components are combined nearly destructively. Because of the cross-phase and cross-gain modulation, the probe light component within the  $\Delta t$ -long time zone survives. The other components outside the  $\Delta t$ -long time zone are removed by the MZI. By adjusting the delay time  $\Delta t$  of the MZI to a time close to the width of the input pulse ( $\lambda_1$ ), the width of the gated pulse ( $\lambda_2$ ) can be made to match that of the input. As a result, each of the input pulses ( $\lambda_1$ ) generates a gated pulse ( $\lambda_2$ ). The co-propagating input pulses ( $\lambda_1$ ) are removed by the bandpass filter after the MZI.

If we ignore the second slowest relaxation of the carrier density in the conventional scheme's gate model, the carrier density is assumed to follow the rate equation,

$$\frac{d}{dt} n(t) = \frac{I_{op}}{qV} - \frac{n(t)}{\tau_1} - \frac{1}{V} \{G(n(t)) - 1\} \times \frac{|E_{pulse}(t)|^2 + |E_{cw}|^2}{\hbar\omega}, \quad (1)$$

where  $n(t)$  is the excess carrier density [5],  $I_{op}$  is the operating current,  $\tau_1$  is the slowest relaxation time constant, and  $G(n(t))$  is the temporal gain.  $E_{pulse}(t)$  and  $E_{cw}$  are the amplitudes of the input pulse ( $\lambda_1$ ) and cw probe light ( $\lambda_2$ ), respectively.

When assuming the second slowest relaxation (such as carrier-cooling relaxation), we incorporate it into our gate model in the simplest manner:

$$\frac{d}{dt}n(t) = \frac{I_{op}}{qV} - \frac{n(t)}{\tau_1} - \frac{1}{V} \{G(n(t)) - 1\} \times \frac{|E_{pulse}(t)|^2 + |E_{cw}|^2}{\hbar\omega},$$

when  $n_{trans} < n(t) < n_{max}$ ,

(2)

and

$$\frac{d}{dt}n(t) = \frac{I_{op}}{qV} - \frac{n(t)}{\tau_2} - \frac{1}{V} \{G(n(t)) - 1\} \times \frac{|E_{pulse}(t)|^2 + |E_{cw}|^2}{\hbar\omega},$$

when  $0 < n(t) < n_{trans}$ .

(3)

Here,  $\tau_2$  is the time constant of the second slowest relaxation,  $n_{max}$  is the saturation level of the carrier density without any optical input light, and  $n_{trans}$  is a transition carrier density that appears to define the threshold between the two relaxation regimes. The dependences of the temporal gain  $G(n(t))$  (ie., XGM) of the SOA and the temporal phase shift  $\Phi_{cw}(t)$  (ie., XPM) of the propagating cw light  $E_{cw}$  on the carrier density were assumed in the simplest manner [Refs. 3 and 5], too:

$$G(n(t)) = \exp\left[\frac{dg}{dn} \cdot n(t) \cdot \Gamma L\right], \text{ and} \quad (4)$$

$$\Phi_{cw}(t) = k_0 \cdot \frac{dn_r}{dn} \cdot [n_{max} - n(t)] \cdot \Gamma L. \quad (5)$$

Here,  $n_r$  is the effective refractive index of the SOA, with respect to the propagating cw light.

Finally, the complex amplitude  $E_{out}(t)$  of the output signal ( $\lambda_2$ ) gated by either of the two alternative DISC schemes in Fig. 1 was expressed as,

$$E_{out}(t) = \frac{1}{\sqrt{2\pi}} \int_{-\infty}^{+\infty} S_{out}(\Delta f) \cdot e^{-i2\pi\Delta f \cdot t} \cdot d(\Delta f). \quad (6)$$

The spectral components before and after the spectral filter (ie., either the MZI or the spectral synthesizer block) are described in the standard manner:

$$S_{out}^{SOA}(\Delta f) = \frac{1}{\sqrt{2\pi}} \int_{-\infty}^{+\infty} E_{cw} \cdot \sqrt{G(n(t))} \cdot e^{i\Phi_{cw}(t)} \cdot e^{+i2\pi\Delta f \cdot t} \cdot dt, \text{ and} \quad (7)$$

$$S_{out}(\Delta f) = S_{out}^{SOA}(\Delta f) \cdot \sqrt{T_f(\Delta f)} \cdot e^{i\Phi_f(\Delta f)}, \quad (8)$$

where  $T_f(\Delta f)$  is the transmittance spectrum of the filter as a function of the detuning of the optical frequency,  $\Delta f \equiv f - f_{cw}$ .  $\Phi_f(\Delta f)$  is the phase profile of the filter.

### 3. Calculated results

Figures 2(a) to (c) respectively show a typical set of the input clock pulse train ( $\lambda_1$ ), the carrier density modulated by the input clock pulses via the SOA, and the gated waveform ( $\lambda_2$ ) in the conventional DISC scheme (Fig. 1(a)), where the second slowest relaxation (such as the carrier-cooling relaxation (CCR)) is completely ignored. The carrier density is rapidly depleted by each of the input clock pulses, and then relatively slowly recovers before the next pulse arrives at the SOA. The gated waveform is not distorted (Fig. 2(c)). The width of the gated pulse almost matches that of the input when we set the MZI's delay time  $\Delta t$  to the width of the input pulse according to the above-mentioned working principle in the time domain. The parameters used in these calculations are summarized in Table 1.

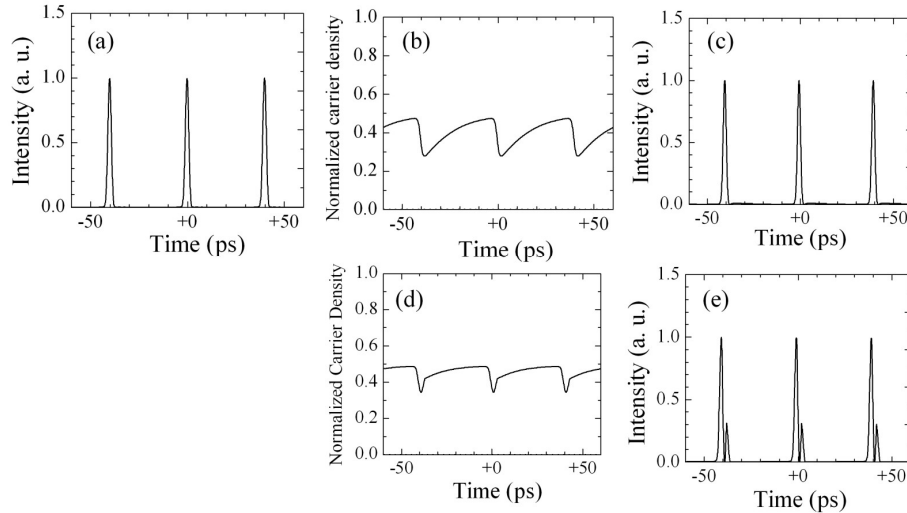


Fig. 2. Calculated probe waveforms all-optically gated via the SOA, by input clock pulses, in the conventional DISC scheme.

(a) Input clock waveform in the time domain, (b) SOA carrier-density evolution without assuming carrier-cooling relaxation (CCR), (c) gated probe waveform without assuming CCR, (d) SOA carrier-density evolution, assuming CCR, and (e) gated probe waveform distortions, assuming CCR.

Table 1. Parameters used in the calculation.

Description	Value
Bit rate, $f_0$	25 Gb/s
Full width at half maximum of input pulse	2.0 ps
Pseudorandom binary data's word length	$2^{31}-1$
Number of data bits in the eye diagram	1,000
Input clock pulse's energy	30 fJ/pulse
Input random-data pulse's energy	30 fJ/pulse
Input cw light power	500 $\mu$ W
Output pulse's width	$\cong 2$ ps
Maximum optical-phase shift after SOA	$0.70\pi$
SOA's slowest time constant, $\tau_1$	50 ps
SOA's second slowest time constant, $\tau_2$ , when assuming CCR	10 ps
Transition carrier density, $n_{\text{trans}}$	$0.42 \times n_{\text{max}}$
SOA's pulse saturation energy	180 pJ
MZI delay time, $\Delta t$	2.0 ps
MZI phase bias, $\Delta\Phi_b$	$1.025\pi$

We can interpret the working principle of the conventional DISC scheme in the frequency domain as follows. Figures 3(a) and 3(b) show the spectral intensity and phase profiles of the cw probe light ( $\lambda_2$ , optical frequency,  $f_{cw} = \frac{c}{\lambda_2}$ ) after it is all-optically cross-gain-modulated

and cross-phase-modulated by the incoming clock pulse train ( $\lambda_1$ ) inside the SOA. These complex spectral profiles were calculated from the complex amplitude of the modulated probe component as a function of time, according to Eq. (7), using a standard fast-Fourier-transformation (FFT) subroutine. Figures 3(c) and (d) show the spectral intensity and phase profiles of the MZI spectral filter's transmissivity, taking its optimum phase bias setting ( $\Delta\Phi_b$ ) into account. After the modulated probe light in Figs. 3(a) and 3(b) is transmitted through the MZI filter in Figs. 3(c) and 3(d), the envelope of intensity profile of the modulated probe light is re-shaped to a smooth and almost Gaussian curve (Fig. 3(e)). The envelope of its phase profile is re-shaped into an almost linear curve (i.e., linearly chirped, excluding the small anomaly near the center frequency) as shown in Fig. 3(f). These complex spectral profiles in Figs. 3(e) and 3(f) are consistent with the clean gated waveform (Fig. 2(c)) generated after the conventional DISC scheme.

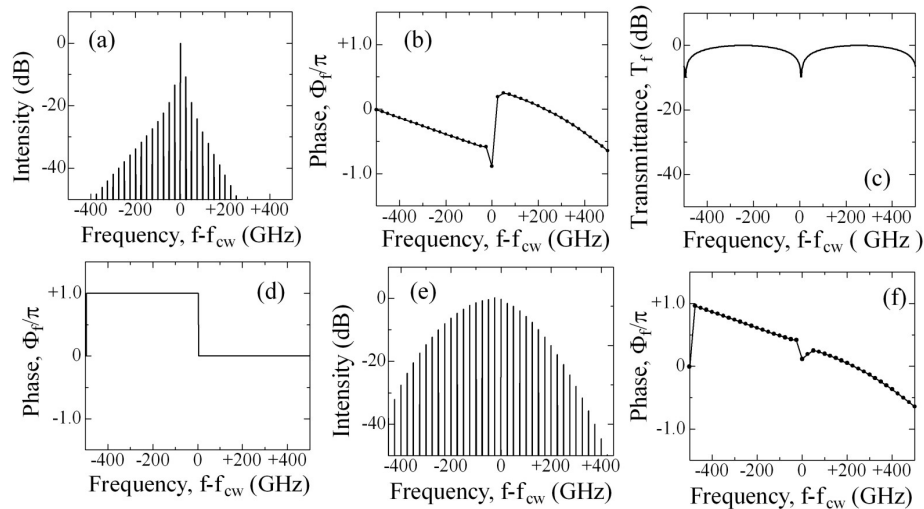


Fig 3. Transitions of calculated optical spectra from input through output, in the conventional scheme without assuming CCR in the SOA.

(a) Intensity profile of a probe's spectral components after the SOA, (b) phase profile of probe's spectral components after the SOA, (c) transmittance spectrum of the MZI filter, (d) phase profile of the MZI filter, (e) intensity profile of the spectral components of the gated probe, (f) phase profile of the spectral components of the gated probe.

In the next step of this work, we took into account the second slowest relaxation, such as CCR, with Eqs. (2) and (3). Figure 2(d) shows an example of the calculated carrier-density evolution, and Fig. 2(e) shows the calculated gated waveform still with the conventional DISC scheme. In this example, we intentionally chose a set of model parameters (Table 1) that ensured the calculated carrier-density would clearly recover with the second slowest time constant  $\tau_2$  to some extent in the first step, and then start recovering with the slowest time constant  $\tau_1$  (Fig. 2(d)). (In fact, many of the cross-gain-modulated probe waveforms that we experimentally measured with our cross-correlator with an ultra-short time resolution of 1 to 2 ps consisted of two-step recovery curves similar to those in Fig. 2(d).) Figure 2(e) indicates that the impact of the two-step recovery curve is very strong; it caused a strong distortion in the gated waveform in the figure. As a result, the gated pulse waveform looked like a doublet

pulse. (The shape of this distorted pulse was more sensitive to the MZI phase bias  $\Delta\Phi_b$  than the gated waveform in Fig. 2(c).)

To interpret the source of the above temporal waveform distortion in the frequency domain, we calculated the intensity and phase profiles of the cw probe light after it was cross-gain-modulated and cross-phase-modulated in the SOA (Figs. 4(a) and 4(b)). Comparing these profiles with those in Figs. 3(a) and (b), we see that the second slowest relaxation significantly influenced both of these intensity and phase profiles. The modulated probe light having complex spectral components in Figs. 4(a) and 4(b) was converted into the strongly distorted waveform in Fig. 2(e), after the modulated probe light propagated through the MZI filter (Figs. 3(c) and 3(d)) in the conventional DISC scheme.

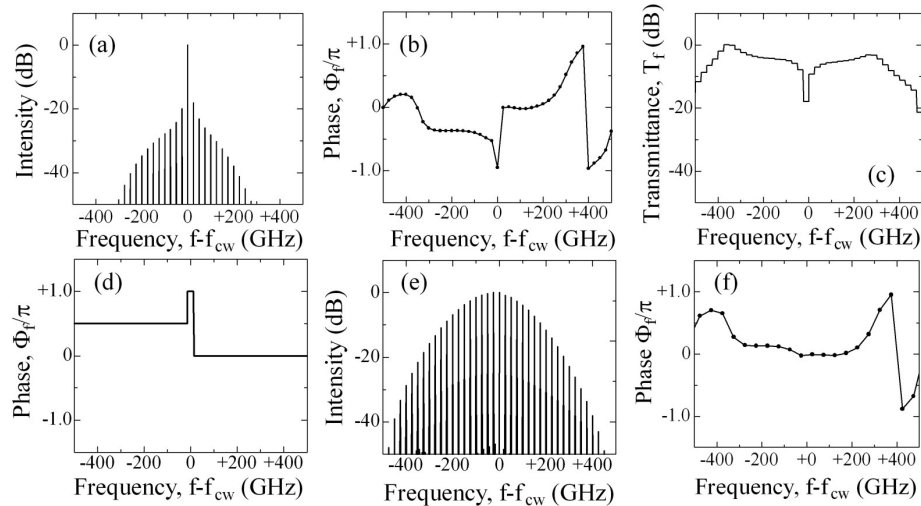


Fig. 4. Transitions of calculated spectra in the expanded DISC scheme, assuming CCR in the SOA.

(a) Intensity profile of probe's spectral components after the SOA, (b) phase profile of probe's spectral components after the SOA, (c) transmittance spectrum design of our optical spectrum synthesizer, (d) phase profile design of our optical spectrum synthesizer, (e) improved intensity profile of the spectral components of a gated probe, and (f) improved phase profile of the spectral components of a gated probe.

Paying attention to the distorted complex spectral components in Figs. 4(a) and (b), we designed the optical spectrum synthesizer in the expanded DISC scheme (Fig. 1(b)) so that the synthesizer compensated for the influences of the second slowest relaxation on the complex spectral components. Figures 4(c) and (d) show the transmittance spectrum and phase profile of the synthesizer, which we came close to optimizing in our manual, step-wise manner. (The synthesizer was assumed to be digital and top-flat, with a frequency resolution matched to the optical pulse frequency of 25 GHz.) After the modulated probe light penetrated the optimized synthesizer, the envelope of the modulated probe light's intensity profile was re-shaped to a smooth, almost Gaussian-like curve (Fig. 4(e)). In addition, the envelope of its phase profile was re-shaped to an almost linear curve within the relative frequency range from  $-300$  GHz to  $+200$  GHz (Fig. 4(f)).

Figures 5(a) to (c) respectively show the set of the input clock pulse train ( $\lambda_1$ ), the carrier density modulated by this input clock train, and the gated waveform ( $\lambda_2$ ) in the expanded DISC scheme that includes the optimized spectrum synthesizer. The gated waveform with very little distortion shown in Fig. 5(c), along with the results in Figs. 4(e) and (f), indicate that the effects of the second slowest relaxation were successfully compensated for by the spectrum synthesizer design in Figs. 4(c) and (d).

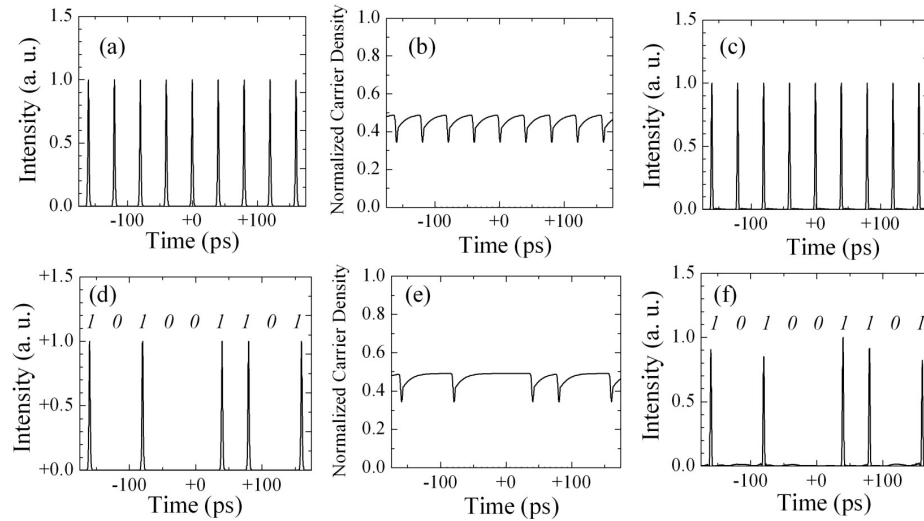


Fig. 5. A gated probe's waveforms at the output of our expanded DISC which includes the optimized spectrum synthesizer from Figs. 4(c) and (d). (a) Input clock pulses, (b) SOA carrier-density modulated by the clock pulses, assuming CCR, (c) probe's intensity waveform gated by the clock pulses, (d) input pseudorandom data pulses, (e) SOA carrier-density modulated by the data pulses, assuming CCR, and (f) probe waveform gated by the data pulses.

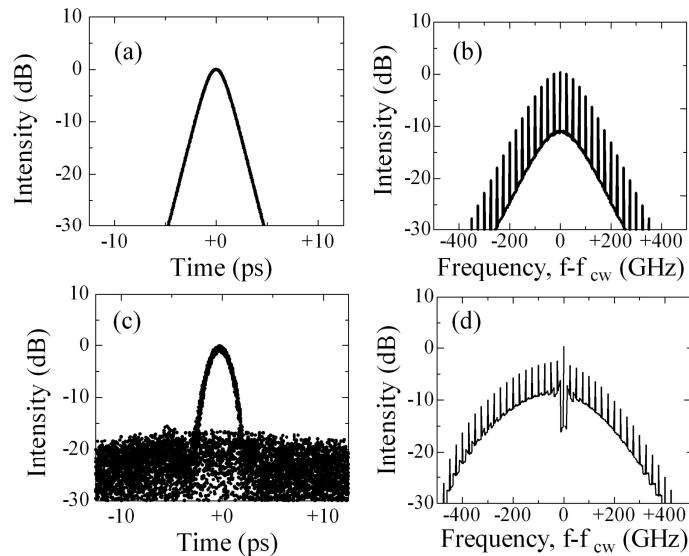


Fig. 6. Pseudorandom data signals before and after our expanded DISC (a) Eye diagram of the input random data signal, (b) optical frequency spectrum of the input random data signal, (c) eye diagram of the gated data signal waveform from Fig. 5(f), and (d) optical frequency spectrum of the gated data signal waveform from Fig. 5(f).

We last investigated whether the above synthesizer design is effective for pseudorandom data pulses in the following ways. Figures 5(d) to (f) respectively show the input data pulse train ( $\lambda_1$ ), the carrier density modulated by the input data pulse train, and the gated waveform ( $\lambda_2$ ). The pseudorandom binary data pattern was numerically generated with a random number generation technique similar to that in [15]. The pattern length was set to  $2^{31}-1$  as that in Ref. 15. The power of the input cw light was increased to 500  $\mu$ W (Table 1) so that the cw light

accelerated the carrier's recovery and consequently suppressed the pattern-induced amplitude fluctuation to within  $\pm 10\%$  in Fig. 5(f). Figures 6(a) and (b) respectively show the eye diagram and averaged optical spectrum of the input random data pulses. Figures 6(c) and (d) respectively show those of the gated waveform in Fig. 5(f). In contrast to the gated waveform that was only partially shown in Fig. 5(f), the eye diagrams in Figs. 6(a) and (c) were generated from 1,000-bit-long random data pulses. The spectra in Figs. 6(b) and (d) were also generated from the same 1,000-bit-long random data pulses. We have three points to make regarding these results:

- a) The gated waveform in Fig. 5(f) indicated that our synthesizer block in the expanded DISC scheme almost fully removed the second-slowest-relaxation-induced distortion from the random data waveform.
- b) In the eye diagram of the gated waveform with the logarithmic intensity scale in Fig. 6(c), the second-slowest-relaxation-induced distortion appeared very weakly, and looked like background noise components. The signal-to-noise ratio in this eye diagram was 20 dB.
- c) The envelope of the frequency spectrum of the gated waveform in Fig. 6(d), excluding the only slightly too strong center-frequency component, was re-shaped as smoothly as that of the gated clock pulses in Fig. 4(e).

#### 4. Discussion

When looking at the wavelength-converted clock pulses in Fig. 5(c), readers might doubt the effectiveness of our synthesizer design: its effectiveness for the clock pulses does not guarantee its effectiveness for real data or equivalently pseudorandom data pulses. The effectiveness for the clock pulses is not innovative, either, because it is mathematically *obvious (self-evident)* from the theorems of the Fourier transformation between a complex temporal waveform and its complex frequency spectrum.

After the preliminary calculation with clock pulses, we numerically tested and confirmed the effectiveness of our design for pseudorandom data pulses from the calculated waveform (Figs. 5(f)), the eye diagram (Fig. 6(c)), and the optical spectrum (Fig. 6(d)). We believe the effectiveness in these respects is *innovative* in our technical community, because it seems difficult or impossible to mathematically prove the quantitative effectiveness indicated in Figs. 5(f), 6(c), and 6(d). Thus, we believe our successful demonstration with the data pulses is evidence of a new and valuable principle.

Furthermore, note that even though we have used a set of model parameters in the 25-GHz frequency range throughout this work, it will be possible to scale-up the characteristic frequency of our synthesizer design closer to and beyond the SOA's transition frequency of 200-300 GHz when more realistically scaling-down the series of characteristic time constants such as the data pulse's distance, width, and the SOA's time constants  $\tau_1$  and  $\tau_2$  after assuming stronger recovery acceleration (or, more advanced, faster optical materials later in the text).

#### 6. Conclusion

We have numerically demonstrated an effective example of optical-spectrum-synthesizer design within the expanded DISC gate scheme; our synthesizer design removed a strong waveform distortion, which was otherwise induced by the second slowest relaxation process (such as the carrier-cooling process) of the SOA inside the DISC gate. The synthesizer design that we digitally optimized with respect to the clock pulse's wavelength conversion proved to be sufficiently effective for conversion of the pseudorandom-digital data pulse's wavelength. We believe it is possible to *generalize* this spectrum-synthesizer design to other types of ultrafast all-optical semiconductor gate designs such as optical demultiplexers, XOR gates, and 3R regenerators for use in sub-Terahertz frequency ranges.

For experimentally testing our synthesizer design in this work, the experimental synthesizer block in Ref. 9 ( $\Delta f \cong 90\text{GHz}$ ) that consisted of MEMS mirrors, spatial lenses, and a conventional grating will be helpful. For developing more practical, volume-production DISC gates in contrast, a monolithically integrated (or hybrid-integrated) *tunable* arrayed-

waveguide grating ( $\Delta f \cong 40\text{GHz}$  in Ref. 16) will be a good candidate of their synthesizer part from the present authors' viewpoint.

Furthermore, we anticipate that this kind of passive-optical-circuit-level design will open a new door to future optical-signal-processing technology, independently of the material-research-level activities aimed at cleaning up higher-order relaxation processes in ultrafast optical materials. For instance, most *quantum-dot* semiconductors, *inter-sub-band-transition* semiconductors, and other ultrafast optical materials now under study tend to contain more than one time constant, including that from their carrier-capture process. We expect the passive-optical-circuit-level design in this work to support development of ultrafast materials for use in industrial logic gate applications, in a manner similar to the base-bias resistors that have supported the electronic transistor element for use in industrial "amplifier" applications since the 1950s.

### **Acknowledgments**

We thank Dr. Mads L. Nielsen for his constructive comments in the early stage of this work in 2005. This work was supported by the research project grant #B15360027 in FY2003-2005, "*Optical logic gates in the sub-Terahertz frequency region*," of the Ministry of Education (MEXT), the research project grant, "*Ultra-low-power and ultrafast optical memory/switching device*," of the New Energy and Industrial Technology Development Organization (NEDO), and the 21st-century University's Center of Excellence (COE) program in FY2003-2007, "*Innovation in coherent optical science*," in the University of Electro-Communications, Japan.